RSC Advances

PAPER

View Article Online
View Journal | View Issue

Cite this: *RSC Adv.*, 2023, **13**, 8220

Construction of defected MOF-74 with preserved crystallinity for efficient catalytic cyanosilylation of benzaldehyde†

Chul Hwan Shim,‡ Sojin Oh,‡ Sujeong Lee, Gihyun Lee and Moonhyun Oh *

Numerous open metal sites and well-developed micropores are the two most significant characteristics that should be imparted to design metal–organic frameworks (MOFs) as effective catalysts. However, the construction of the best MOF catalyst with both these characteristics is challenging because the creation of numerous open metal sites generally triggers some structural collapse of the MOF. Herein, we report the construction of well-structured but defected MOFs through the growth of defected MOFs, where some of the original organic linkers were replaced with analog organic linkers, on the surface of a crystalline MOF template (MOF-on-MOF growth). Additional open metal sites within the MOF-74 structure were generated by replacing some of the 2,5-dihydroxy-1,4-bezenedicarboxylic acid presenting in MOF-74 with 1,4-benzenedicarboxylic acid due to the missing hydroxyl groups. And the resulting additional open metal sites within the MOF-74 structure resulted in enhanced catalytic activity for the cyanosilylation of aldehydes. However, the collapse of some of the well-developed MOF-74 structure was also followed by structural defects. Whereas, the growth of defected MOF-74 (D-MOF-74) on the well-crystallized MOF-74 template led to the production of relatively well-crystallized D-MOF-74. Core–shell type MOF-74@D-MOF-74 having abundant open metal sites with a preserved crystallinity exhibited the efficient catalytic cyanosilylation of several aldehydes. Additionally, MOF-74@D-MOF-74 displayed excellent recyclability during the consecutive catalytic cycles.

Received 23rd February 2023
Accepted 3rd March 2023

DOI: 10.1039/d3ra01222k

rsc.li/rsc-advances

Introduction

Metal–organic frameworks (MOFs) are an important class of porous crystalline materials used in various practical applications, including gas storage, recognition, sensing, separation, and catalysis.[1–6] In particular, the use of MOFs in catalysis has received considerable attention and the design of MOFs to yield excellent activity is critical for their practical applications.[7–17] Well-defined channels or pores in MOFs are beneficial for their excellent catalytic activity, and unsaturated Lewis acid metal sites (open metal sites) are known to be active sites for the catalytic reactions.[8–17] There are several approaches to generate additional open metal sites within an MOF structure for improved catalytic activity.[11–17] Removing some of the existing organic linkers in an original MOF structure can generate extra open metal sites, just as replacing some of them with analog linkers having fewer coordination sites can also generate extra open metal sites. For example, Eder *et al.* reported the generation of defected MIL-125 with open metal sites through removing some of the 2-amino-1,4-benzenedicarboxylic acid within an MIL-125 structure,[13] and Li *et al.* reported the production of defected CoBDC-Fc by replacing some of the 1,4-benzenedicarboxylic acid (BDC) linker by ferrocenecarboxylic acid.[11] However, in most cases of producing defected MOFs with extra open metal sites, removing or replacing the original organic linkers has resulted in structural defects and instability.[16–20] In such cases, the MOFs consequently lose some of their crystallinity, resulting in lowered catalytic activity as excessive defects and poor crystallinity in MOFs interrupt smooth chemical transportation during catalytic reactions.[15–17] Therefore, the construction of defected MOFs having many open metal sites without losing their crystallinity is most desirable.

Herein, we report the construction of defected MOFs having extra open metal sites with preserved crystallinity through the growth of defected MOFs on the crystalline MOF template (MOF-on-MOF growth). Replacing some of the 2,5-dihydroxy-1,4-bezenedicarboxylic acid (DHBDC) within the MOF-74 structure with BDC resulted in defected MOF-74 (D-MOF-74) having additional open metal sites owing to the missing hydroxyl groups. The resulting extra open metal sites within defected MOFs caused the enhancement of catalytic activity for the cyanosilylation of benzaldehyde. However, structural

Department of Chemistry, Yonsei University, 50 Yonsei-ro, Seodaemun-gu, Seoul 03722, Republic of Korea. E-mail: moh@yonsei.ac.kr; Fax: +82-2-364-7050; Tel: +82-2-2123-5637

† Electronic supplementary information (ESI) available. See DOI: https://doi.org/10.1039/d3ra01222k

‡ These authors contributed equally to this article.

defects also caused the collapse of the well-organized MOF-74 structure, negatively impacting the catalytic reaction. Whereas the directed growth of D-MOF-74 on the surface of the well-crystallized MOF-74 template led to the formation of relatively well-crystallized D-MOF-74 shell. Eventually, core–shell type MOF-74@D-MOF-74 with abundant open metal sites and a preserved well-developed porosity displayed the best performance for the cyanosilylation of several aldehydes. Moreover, they exhibited excellent recyclability during seven successive catalytic cycles.

Experimental

Materials and characterizations

All solvents and chemicals were purchased from commercial sources and used as received, unless otherwise stated. SEM images were captured using a JEOL JSM-7001F field-emission SEM (Yonsei Center for Research Facilities, Yonsei University). EDX spectra were acquired using a Hitachi SU 1510 SEM equipped with a Horiba EMAX Energy E-250 EDX system. PXRD patterns were obtained using a Rigaku Ultima IV equipped with a graphite monochromated Cu Kα radiation source (40 kV, 40 mA). The adsorption–desorption isotherms of N_2 (77 K) were measured using a BELSORP Max volumetric adsorption instrument. All isotherms of samples were measured after soaking in methanol for 10 h and a pretreatment under a dynamic vacuum at 120 °C for 12 h. ^{1}H NMR spectra were recorded on a Bruker Avance III HD 300 spectrometer (^{1}H NMR, 300 MHz) with chemical shifts reported relative to residual deuterated solvent peaks. TGA curves were acquired using a Shimadzu TGA-50 system under a nitrogen atmosphere at a heating rate of 5 °C min^{-1}. Inductively coupled plasma-mass spectrometer analysis was performed using a PerkinElmer NexION 350D instrument to quantify cobalt in the supernatant after catalytic reaction.

Preparation of MOF-74

$CoCl_2 \cdot 6H_2O$ (0.30 mmol, 71.4 mg), DHBDC (0.075 mmol, 14.9 mg), and polyvinylpyrrolidone (PVP; 250 mg) were dissolved in 5 mL *N*,*N*-dimethylformamide (DMF). The resulting mixture was heated in a 120 °C oil bath for 2 h, then isolated *via* centrifugation, washed with fresh DMF and methanol, and dried in vacuum for 1 h. Large scale production of MOF-74 was also conducted using $CoCl_2 \cdot 6H_2O$ (2.40 mmol, 571.2 mg), DHBDC (0.6 mmol, 119.2 mg), PVP (2 g), and 40 mL DMF.

Preparation of D-MOF-74

$CoCl_2 \cdot 6H_2O$ (0.30 mmol, 71.4 mg), DHBDC (0.01, 0.015, 0.024, or 0.028 mmol), BDC (0.040, 0.060, 0.096, or 0.112 mmol), and PVP (250 mg) were dissolved in 5 mL of DMF. The resulting mixture was placed in a 120 °C oil bath for 2 h, then isolated *via* centrifugation, washed with fresh DMF and methanol, and dried in vacuum for 1 h. The products obtained from four varied concentrations of reactants are denoted as D1-, D2-, D3-, and D4-MOF-74, respectively. Large scale production of D3-MOF-74 was also conducted using $CoCl_2 \cdot 6H_2O$ (2.40 mmol, 571.2 mg), DHBDC (0.192 mmol, 38.4 mg), BDC (0.768 mmol, 127.2 mg), PVP (2 g), and 40 mL DMF.

Preparation of MOF-74@D-MOF-74

$CoCl_2 \cdot 6H_2O$ (0.30 mmol, 71.4 mg), DHBDC (0.01, 0.015, 0.024, or 0.028 mmol), BDC (0.040, 0.060, 0.096, or 0.112 mmol), and PVP (250 mg) were dissolved in 5 mL of DMF. 4.0 mg of MOF-74 was added to the resulting mixture, and the resulting suspension was placed in a 120 °C oil bath for 2 h, then isolated *via* centrifugation, washed with fresh DMF and methanol, and dried in vacuum for 1 h. Large scale production of MOF-74@D3-MOF-74 was also conducted using $CoCl_2 \cdot 6H_2O$ (2.40 mmol, 571.2 mg), DHBDC (0.192 mmol, 38.4 mg), BDC (0.768 mmol, 127.2 mg), PVP (2 g), MOF-74 (32.0 mg), and 40 mL DMF.

Cyanosilylation of benzaldehyde

Benzaldehyde (1 mmol), trimethylsilyl cyanide (TMSCN; 3 mmol), and MOF catalyst (MOF-74, D-MOF-74, or MOF-74@D-MOF-74; 3.0 mg) were mixed in a 4 mL vial. The resulting mixture was reacted at 60 °C for 30 min with constant stirring. After 30 min, the catalyst was isolated *via* centrifugation, and ^{1}H NMR spectra were measured to determine the conversion of benzaldehyde. Similar cyanosilylation reactions were also conducted using 4-methoxybenzaldehyde, 4-methylbenzaldehyde, and 4-fluorobenzaldehyde instead of benzaldehyde. For the recycling test, seven cycles of benzaldehyde cyanosilylation were repeated with the MOF-74@D2-MOF-74 (or D3-MOF-74) catalyst. After the first catalytic reaction, the catalyst was isolated *via* centrifugation, washed with methanol several times, and dried under vacuum for 1 h. Subsequently, fresh benzaldehyde and TMSCN were added into the vial containing the refreshed catalyst for a second catalytic cycle. The same procedure was repeated for a seventh catalytic cycle.

Results and discussion

Firstly, a three-dimensional (3D) hexagonal structured MOF (MOF-74) with a chemical composition of $[Co_2(DHBDC)(H_2O)_2]_n$ was synthesized from the solvothermal reaction of $CoCl_2$ and DHBDC (Scheme 1 and Fig. S1, ESI†).[21] Scanning electron microscopy (SEM) image (Fig. 1a) of the resulting product revealed the uniform production of hexagonal rods with a high aspect ratio, and powder X-ray diffraction (PXRD) patterns (Fig. 1d) of the product, which matched the representative PXRD pattern of MOF-74, confirmed the production of well-crystallized MOF-74. Next, defected MOF-74 (denoted as D-MOF-74; $[Co_2(DHBDC)_{1-x}(BDC)_x(H_2O)_2Y_z]_n$) was prepared *via* similar solvothermal reactions of $CoCl_2$, but in the presence of two organic linkers, DHBDC and BDC (the products obtained from four varied concentrations of reactants are denoted as D1-, D2-, D3-, and D4-MOF-74, respectively. See experimental section for details). The incorporation of BDC instead of some of the original DHBDC within an MOF-74 structure should invoke structural defects owing to the missing hydroxyl moieties within the structure (Scheme 1 and Fig. S2, ESI†). Typically, hydroxyl groups and carboxyl groups of DHBDC are coordinated to metal

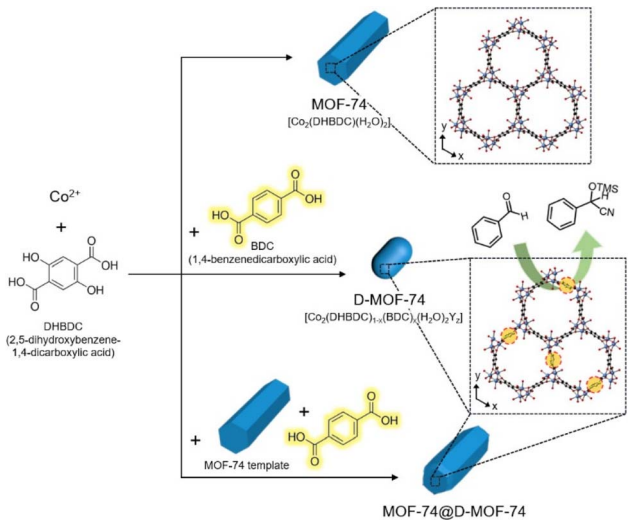

Scheme 1 Schematic of the synthesis of MOF-74, D-MOF-74, and core–shell type MOF-74@D-MOF-74.

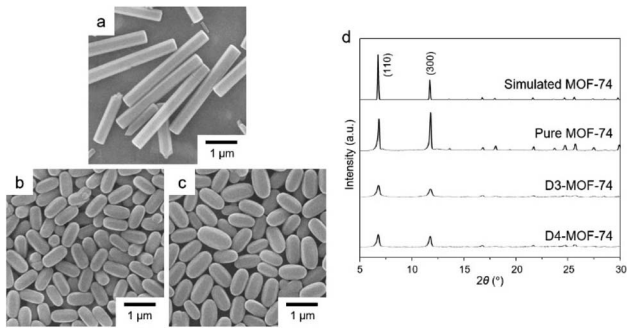

Fig. 1 SEM images of (a) pure MOF-74, (b) D3-MOF-74, and (c) D4-MOF-74. (d) PXRD patterns of pure MOF-74, D3-MOF-74, and D4-MOF-74. The simulated PXRD pattern of MOF-74 is also shown.

ions to form the CoO_6 octahedra of an MOF-74 structure (Fig. S1, ESI†);[22] thus, the missing hydroxyl moieties should result in additional open metal sites (Fig. S2, ESI†) within the MOF-74 structure that should be beneficial for its catalytic activity. The additional open metal sites provoked from the missing hydroxyl moieties are located toward the hexagonal channels of the MOF-74 structure, as shown in Fig. S3 (ESI†). However, the replacement of some of DHBDC with BDC also causes structural instability owing to the missing hydroxyl moieties, which originally participate in building the MOF-74 skeleton.

The morphologies of the resulting D-MOF-74 were validated through SEM images of the samples. As shown in Fig. 1, the production of rounded ovals was confirmed from the reactions of $CoCl_2$ with the two mixed organic linkers. PXRD patterns of D-MOF-74 samples verified that they principally had a 3D hexagonal MOF-74 structure (Fig. 1d). However, the peaks broadened and decreased,[17,18,23] possibly due to the gradual loss of its crystallinity as BDC is included. In general, rounded MOF particles represent amorphous characteristic of the MOF.[17,24,25] Therefore, the rounded shape of D-MOF-74 samples supported the amorphous nature of defected MOF-74. Energy dispersive X-ray (EDX) spectra of the samples displayed the detection of carbon, oxygen, and cobalt elements, confirming the existence of cobalt ions and organic linkers (Fig. S4, ESI†). In addition, extra anions must be existed in D-MOF-74 for the charge balance due to the incorporation of BDC instead of some of DHBDC. Indeed, EDX spectra of D-MOF-74 samples exhibited the presence of Cl element (Fig. S4, ESI†). Moreover, the incorporated amounts of DHBDC and BDC within D-MOF-74 were analyzed by ^{1}H NMR spectroscopy. D-MOF-74 samples were added to a mixed deuterated solvent of DCl and DMSO-d_6 to digest solid D-MOF-74 samples and measure ^{1}H NMR spectra. The incorporated amounts of BDC within D3-MOF-74 and D4-MOF-74 were found to be 4.6 and 3.5%, respectively (Fig. S5, ESI†). PXRD patterns and ^{1}H NMR spectra of D1-MOF-74 and D2-MOF-74 could not be measured because only trace amounts of D1-MOF-74 and D2-MOF-74 were produced during the reactions at relatively dilute concentrations.

The amounts of D-MOF-74 generated from the reactions were small (calculated yields for D3-MOF-74 and D4-MOF-74 were 21 and 83%, respectively, and the yields for D1-MOF-74 and D2-MOF-74 were less than 3%). In addition, the gradual loss of its crystallinity with the incorporation of BDC was resulted as mentioned before. For a more efficient production of D-MOF-74 with preserving its crystallinity, the similar reactions of $CoCl_2$ with mixed two organic linkers were conducted in the presence of the MOF-74 template to generate D-MOF-74 in the form of core–shell MOF-74@D-MOF-74. The growth of second MOF on the surface of template MOF (MOF-on-MOF growth) has been well established for the conjugation of two different MOFs or the production of unique MOFs.[26–35] Especially, a well-crystallized template MOF can induce the growth of a well-crystallized second MOF.[31–35] The presence of well-crystallized MOF-74 should induce not only the effective growth of D-MOF-74 but also the production of D-MOF-74 with a preserved crystallinity by providing well-ordered lattices to the reactants.[31–35] First, the yields of the reactions dramatically increased in the presence of the MOF-74 template. The amounts of D-MOF-74 produced were calculated based upon the initial weight of the MOF-74 template and the final weight of MOF-74@D-MOF-74. Even though no meaningful formation (less than 3%) of D1-MOF-74 and D2-MOF-74 was observed without the template, considerable amounts of D1-MOF-74 (53%) and D2-MOF-74 (60%) were produced on the surface of the MOF-74 template. In addition, the yields of D3-MOF-74 and D4-MOF-74 were 82 and 78%, respectively. SEM images (Fig. 2) of the resulting products revealed that the hexagonal MOF-74 shape was well maintained even after a MOF-on-MOF growth process for the production of core–shell MOF-74@D-MOF-74. In addition, progressively increased widths of hexagonal rods were obviously detected in SEM images of a series of MOF-74@D-MOF-74 samples (Fig. 2). PXRD patterns of a series of MOF-74@D-MOF-74 samples displayed the representative peaks for MOF-74 (Fig. 2f). In addition, there was no significant peak broadening after D-MOF-74 formation on the surface of MOF-74 template, indicating no

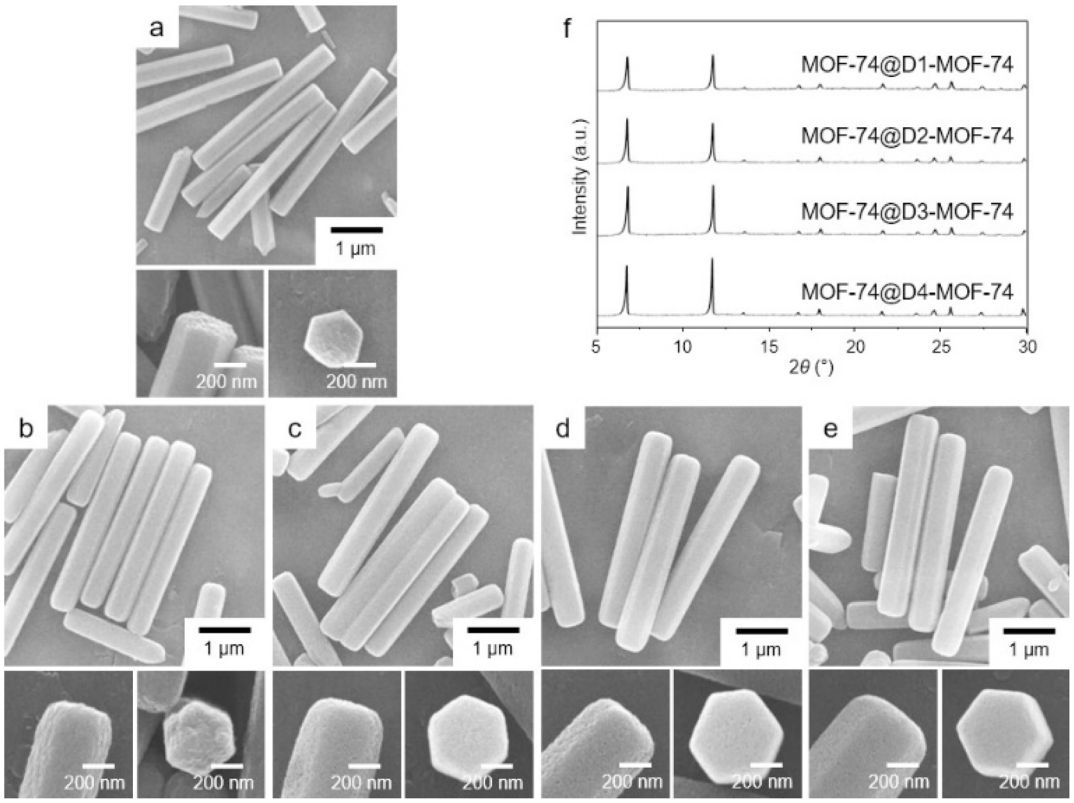

Fig. 2 SEM images of (a) MOF-74 template, (b) MOF-74@D1-MOF-74, (c) MOF-74@D2-MOF-74, (d) MOF-74@D3-MOF-74, and (e) MOF-74@D4-MOF-74. (f) PXRD patterns of a series of MOF-74@D-MOF-74.

critical loss of its crystallinity in MOF-74@D-MOF-74. The incorporated amounts of BDC within the D-MOF-74 shell were calculated based on their ^{1}H NMR spectra and the relative amounts of the MOF-74 core and the D-MOF-74 shell within MOF-74@D-MOF-74. The calculations indicated that the incorporated amounts of BDC within the D-MOF-74 shell of MOF-74@D-MOF-74 were 20.8, 5.9, 3.0, and 2.2%, respectively (Fig. S6, ESI†). Meanwhile, large scale productions of D-MOF-74 and MOF-74@D-MOF-74 were also successful using large amounts of reactants (Fig. S7, ESI†).

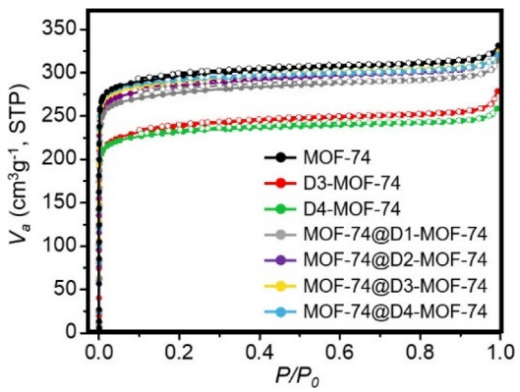

Fig. 3 N_2 sorption isotherms of MOF-74, a series of D-MOF-74, and a series of MOF-74@D-MOF-74.

The porosities of the D-MOF-74 and MOF-74@D-MOF-74 samples were then analyzed from their N_2 sorption isotherms (Fig. 3). Brunauer–Emmett–Teller (BET) surface areas and total pore volumes of the D-MOF-74 samples prepared in the absence of template decreased compared to those of pure MOF-74. The BET surface area and total pore volume of pure MOF-74 were 1180.8 m^2 g^{-1} and 0.50 cm^3 g^{-1}, respectively, whereas the BET surface areas of D3-MOF-74 and D4-MOF-74 were 925.7 and 919.3 m^2 g^{-1} and their total pore volumes were 0.43 and 0.40 cm^3 g^{-1}, respectively. These decreasing values of D-MOF-74 are originated from some structural collapse and a gradual loss of its crystallinity as the DHBDC linker is replaced with the BDC linker. However, no significant decreases in N_2 sorption, BET surface area, and total pore volume were observed in the MOF-74@D-MOF-74 samples (Fig. 3 and Table S1, ESI†). For examples the BET surface areas of MOF-74@D3-MOF-74 and MOF-74@D4-MOF-74 were 1158.9 and 1172.3 m^2 g^{-1} and their total pore volumes were 0.50 and 0.50 cm^3 g^{-1}, respectively. In addition, the relative values of the D-MOF-74 shells within a series of MOF-74@D-MOF-74 were estimated based on the relative amounts of the MOF-74 core and the D-MOF-74 shell. The estimated BET surface areas of D3-MOF-74 and D4-MOF-74 within MOF-74@D-MOF-74 samples were 1146.4 and 1167.9 m^2 g^{-1} and their total pore volumes estimated were 0.50 and 0.50 cm^3 g^{-1}, respectively (Table S2, ESI†). These values are higher than those of the corresponding D-MOF-74 generated without the template. In addition, no critical difference was found in the

pore size distributions of pure MOF-74 and MOF-74@D-MOF-74 calculated using non-local density functional theory (Fig. S8, ESI†). No difference in thermal stability of pure MOF-74 and MOF-74@D-MOF-74 was also detected in the thermogravimetric analysis curves (Fig. S9, ESI†).

The improvement of the catalytic activity of the D-MOF-74 samples through providing additional open metal sites, which can function as Lewis acid catalytic sites, was verified from their enhanced activity on the cyanosilyation of benzaldehyde. Cyanosilylation of aldehydes is significant because it is a critical method to synthesize cyanohydrins, which are key compounds for the synthesis of several fine chemicals, including pharmaceuticals.[36–38] Benzaldehyde and trimethylsilyl cyanide (TMSCN) were reacted in the presence of a catalytic amount of pure MOF-74 or a series of D-MOF-74 under solvent-free conditions at 60 °C for 30 min (Table 1). After the reactions, ^{1}H NMR spectroscopy was used to determine the conversion of benzaldehyde to 2-phenyl-2-[(trimethylsilyl)oxy] acetonitrile in the absence or presence of an internal standard (Tables 1, S3, and Fig. S10, ESI†). The conversion of benzaldehyde in the presence of D-MOF-74 was much higher than that in the presence of pure MOF-74. Pure MOF-74 displayed 65% conversion of the initial benzaldehyde for 30 min; however, 93 and 92% conversions were observed in the presence of D3-MOF-74 and D4-MOF-74, respectively. The catalytic activity of MOF-74 was enhanced up to 28% by replacing only 4.6% of DHBDC with BDC. MOF-74@D3-MOF-74 and MOF-74@D4-MOF-74 also exhibited enhanced conversion efficiency at 93 and 91%, respectively. However, when the actual amount of D-MOF-74 within MOF-74@D-MOF-74 is considered, the catalytic activity of D-MOF-74 in MOF-74@D-MOF-74 is more dramatically enhanced compared to that of D-MOF-74 generated without the template. In fact, only 1.9% of the BDC was incorporated within MOF-74@D3-MOF-74. MOF-74@D2-MOF-74, where 2.7% of the BDC was incorporated, displayed a best catalytic activity with 96% conversion. Conserving its crystallinity during the construction of D-MOF-74 due to the efficient guide of well-crystallized MOF-74 is a reason for the improvement of catalytic activity of D-MOF-74 within MOF-74@D-MOF-74. The plots for the conversions of benzaldehyde to 2-phenyl-2-[(trimethylsilyl)oxy] acetonitrile by pure MOF-74 and MOF-74@D2-MOF-74 in varied time points were also obtained as shown in Fig. S11a (ESI†). Moreover, a linear relationship between $\ln(C_t/C_0)$ and the reaction time was observed, which revealed first-order reaction kinetics (Fig. S11b, ESI†).[39,40]

Meanwhile, cobalt ions can bleach out from the catalyst during the catalytic reaction; however, no critical bleaching of cobalt ions from the catalyst (MOF-74@D2-MOF-74) was found during the catalytic reaction. Inductively coupled plasma-mass spectrometer analysis revealed that *ca.* 0.8% of cobalt bleached out from the catalyst after the catalytic reaction. Control experiments for cyanosilylation of benzaldehyde were also conducted. Cyanosilylation of benzaldehyde without any catalyst was occurred but showed very low activity.[41–43] And the salt ($CoCl_2$) was also active for cyanosilylation of benzaldehyde under homogeneous condition, as already known.[41–43] Moreover, cyanosilylation reactions of three other aldehydes, such as 4-methoxybenzaldehyde, 4-methylbenzaldehyde, and 4-fluorobenzaldehyde were performed in the presence of a catalytic amount of pure MOF-74 and MOF-74@D2-MOF-74 (Fig. S12–S14, ESI†). In general, the catalytic activity of MOF-74@D2-MOF-74 was higher than that of pure MOF-74 for the cyanosilylation of three aldehydes (Table 2). The cyanosilylation of aldehyde having electron donating groups is normally faster than that of aldehyde bearing electron withdrawing groups.[44,45]

Table 1 Cyanosilylation of benzaldehyde with TMSCN catalyzed by pure MOF-74, a series of D-MOF-74, and a series of MOF-74@D-MOF-74[a]

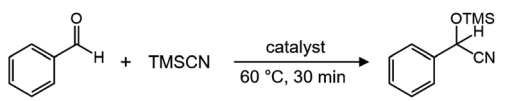

Entry	Catalyst	Conversion (%)
1	MOF-74	65
2	D3-MOF-74	93
3	D4-MOF-74	92
4	MOF-74@D1-MOF-74	89
5	MOF-74@D2-MOF-74	96
6	MOF-74@D3-MOF-74	93
7	MOF-74@D4-MOF-74	91

[a] Reaction conditions: benzaldehyde (1 mmol), MOF catalyst (3.0 mg, 1.7 mol% based on Co(II)), trimethylsilyl cyanide (TMSCN; 3 mmol).

Table 2 Cyanosilylation of various aldehydes with TMSCN catalyzed by pure MOF-74 and MOF-74@D2-MOF-74[a]

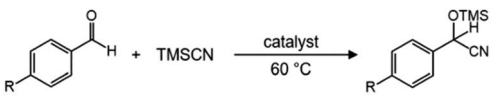

Entry	Substrate	Time (min)	Conversion (%) MOF-74	Conversion (%) MOF-74@D2-MOF-74
1	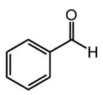	30	65	96
2	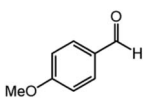	10	61	79
3	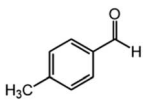	30	61	95
4	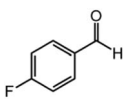	30	63	79

[a] Reaction conditions: aldehyde (1 mmol), MOF catalyst (3.0 mg, 1.7 mol% based on Co(II)), trimethylsilyl cyanide (TMSCN; 3 mmol).

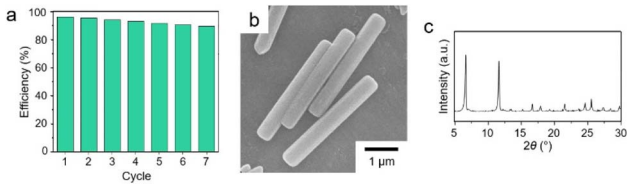

Fig. 4 (a) Recyclability of MOF-74@D2-MOF-74 over seven successive catalytic cycles. (b) SEM image and (c) PXRD pattern of MOF-74@D2-MOF-74 after seven successive catalytic reactions.

The recyclability of the catalyst was examined using MOF-74@D2-MOF-74 and D3-MOF-74. The cyanosilyation activity was well maintained even after seven successive catalytic cycles (Fig. 4). Moreover, the SEM image and PXRD pattern of MOF-74@D2-MOF-74 after seven catalytic cycles verified no critical morphological change and no structural change even after seven successive catalytic reactions (Fig. 4). D3-MOF-74 also exhibited good recyclability as shown in its catalytic activity during seven successive catalytic reactions (Fig. S15, ESI†).

Conclusions

In conclusion, two series of defected MOF-74 were successfully prepared by replacing a small amount of DHBDC linker originally present in MOF-74 with BDC linker. Owing to the missing hydroxyl groups in the BDC linker compared to the DHBDC linker, extra open metal sites were produced within the D-MOF-74 structure. Two series of D-MOF-74 were prepared from a series of reactions in the absence or presence of the MOF-74 template. All the resulting D-MOF-74 displayed an enhanced catalytic activity for the cyanosilyation of benzaldehyde compared to that of pure MOF-74. D-MOF-74 generated in the absence of the MOF-74 template was found to lose its crystallinity. On the other hand, the well-crystallized MOF-74 template invoked a more efficient growth of D-MOF-74 without losing its crystallinity. Finally, core–shell type MOF-74@D-MOF-74 with many open metal sites and preserved well-developed porosity exhibited the best performance as a catalyst. Moreover, excellent recyclability was demonstrated during several consecutive catalytic reactions. The synthetic approach suggested here for the production of defected MOFs having many open metal sites with preserved original porosity should be beneficial in the development of highly active MOFs applicable in catalysis, sensing, and adsorption.

Author contributions

Moonhyun Oh designed, coordinated the research, and drafted the manuscript. Chul Hwan Shim, Sojin Oh, Sujeong Lee, and Gihyun Lee conducted experiments and data analysis. Sojin Oh, Sujeong Lee, Gihyun Lee, and Moonhyun Oh revised the manuscript. The authors read and approved the final manuscript.

Conflicts of interest

There are no conflicts to declare.

Acknowledgements

This research was supported by the Challengeable Future Defense Technology Research and Development Program through the Agency for Defense Development (ADD) funded by the Defense Acquisition Program Administration (DAPA) in 2022 (No. 915019201).

Notes and references

1 M. Bonneau, C. Lavenn, J. J. Zheng, A. Legrand, T. Ogawa, K. Sugimoto, F. X. Coudert, R. Reau, S. Sakaki, K. Otake and S. Kitagawa, *Nat. Chem.*, 2022, **14**, 816–822.
2 L. Li, R. B. Lin, R. Krishna, H. Li, S. Xiang, H. Wu, J. Li, W. Zhou and B. Chen, *Science*, 2018, **362**, 443–446.
3 T. Y. Luo, P. Das, D. L. White, C. Liu, A. Star and N. L. Rosi, *J. Am. Chem. Soc.*, 2020, **142**, 2897–2904.
4 R. L. Siegelman, E. J. Kim and J. R. Long, *Nat. Mater.*, 2021, **20**, 1060–1072.
5 J. Liu, T. A. Goetjen, Q. Wang, J. G. Knapp, M. C. Wasson, Y. Yang, Z. H. Syed, M. Delferro, J. M. Notestein, O. K. Farha and J. T. Hupp, *Chem. Soc. Rev.*, 2022, **51**, 1045–1097.
6 H. Yoon, S. Lee, S. Oh, H. Park, S. Choi and M. Oh, *Small*, 2019, **15**, 1805232.
7 F. Zhang, J. Zhang, B. Zhang, L. Zheng, X. Cheng, Q. Wan, B. Han and J. Zhang, *Green Chem.*, 2020, **22**, 5995–6000.
8 Y. Wen, J. Zhang, Q. Xu, X. T. Wu and Q. L. Zhu, *Coord. Chem. Rev.*, 2018, **376**, 248–276.
9 Y. Shen, T. Pan, L. Wang, Z. Ren, W. Zhang and F. Huo, *Adv. Mater.*, 2021, **33**, 2007442.
10 S. Dissegna, K. Epp, W. R. Heinz, G. Kieslich and R. A. Fischer, *Adv. Mater.*, 2018, **30**, 1704501.
11 Z. Xue, K. Liu, Q. Liu, Y. Li, M. Li, C. Y. Su, N. Ogiwara, H. Kobayashi, H. Kitagawa, M. Liu and G. Li, *Nat. Commun.*, 2019, **10**, 5048.
12 G. Cai and H. L. Jiang, *Angew. Chem., Int. Ed.*, 2017, **56**, 563–567.
13 S. Naghdi, A. Cherevan, A. Giesriegl, R. Guillet-Nicolas, S. Biswas, T. Gupta, J. Wang, T. Haunold, B. C. Bayer, G. Rupprechter, M. C. Toroker, F. Kleitz and D. Eder, *Nat. Commun.*, 2022, **13**, 282.
14 H. Jiang, Q. Wang, H. Wang, Y. Chen and M. Zhang, *ACS Appl. Mater. Interfaces*, 2016, **8**, 26817–26826.
15 Z. Fan, J. Wang, W. Wang, S. Burger, Z. Wang, Y. Wang, C. Wöll, M. Cokoja and R. A. Fischer, *ACS Appl. Mater. Interfaces*, 2020, **12**, 37993–38002.
16 Z. Jiang, L. Ge, L. Zhuang, M. Li, Z. Wang and Z. Zhu, *ACS Appl. Mater. Interfaces*, 2019, **11**, 44300–44307.
17 H. Jun, S. Oh, G. Lee and M. Oh, *Sci. Rep.*, 2022, **12**, 14735.
18 O. Kozachuk, I. Luz, F. X. Llabrés i Xamena, H. Noei, M. Kauer, H. B. Albada, E. D. Bloch, B. Marler, Y. Wang, M. Muhler and R. A. Fischer, *Angew. Chem., Int. Ed.*, 2014, **53**, 7058–7062.
19 A. F. Möslein, L. Donà, B. Civalleri and J. C. Tan, *ACS Appl. Nano Mater.*, 2022, **5**, 6398–6409.

20 A. W. Thornton, R. Babarao, A. Jain, F. Trousselet and F. X. Coudert, *Dalton Trans.*, 2016, **45**, 4352–4359.
21 C. Young, J. Kim, Y. V. Kaneti and Y. Yamauchi, *ACS Appl. Energy Mater.*, 2018, **1**, 2007–2015.
22 P. D. C. Dietzel, Y. Morita, R. Blom and H. Fjellvåg, *Angew. Chem., Int. Ed.*, 2005, **44**, 6354–6358.
23 T. D. Bennett and A. K. Cheetham, *Acc. Chem. Res.*, 2014, **47**, 1555–1562.
24 Z. Gao, B. Xu, Y. Fan, T. Zhang, S. Chen, S. Yang, W. Zhang, X. Sun, Y. Wei, Z. Wang, X. Wang, X. Meng and Y. S. Zhao, *Angew. Chem., Int. Ed.*, 2021, **60**, 6362–6366.
25 H. J. Lee, J. We, J. O. Kim, D. Kim, W. Cha, E. Lee, J. Sohn and M. Oh, *Angew. Chem., Int. Ed.*, 2015, **54**, 10564–10568.
26 L. Chai, J. Pan, Y. Hu, J. Qian and M. Hong, *Small*, 2021, **17**, 2100607.
27 M. Abdollahzadeh, M. Chai, E. Hosseini, M. Zakertabrizi, M. Mohammad, H. Ahmadi, J. Hou, S. Lim, A. H. Korayem, V. Chen, M. Asadnia and A. Razmjou, *Adv. Mater.*, 2022, **34**, 2107878.
28 S. Lee, S. Oh and M. Oh, *Angew. Chem., Int. Ed.*, 2020, **59**, 1327–1333.
29 S. Choi, T. Kim, H. Ji, H. J. Lee and M. Oh, *J. Am. Chem. Soc.*, 2016, **138**, 14434–14440.
30 Y. Wang, Z. Zhang, J. Li, Y. Yuan, J. Yang, W. Xu, P. An, S. Xi, J. Guo, B. Liu and J. Li, *Angew. Chem., Int. Ed.*, 2022, **61**, e202211031.
31 H. Ji, S. Lee, J. Park, T. Kim, S. Choi and M. Oh, *Inorg. Chem.*, 2018, **57**, 9048–9054.
32 S. Lee, G. Lee and M. Oh, *ACS Nano*, 2021, **15**, 17907–17916.
33 G. Lee, S. Lee, S. Oh, D. Kim and M. Oh, *J. Am. Chem. Soc.*, 2020, **142**, 3042–3049.
34 M. Zhao, J. Chen, B. Chen, X. Zhang, Z. Shi, Z. Liu, Q. Ma, Y. Peng, C. Tan, X. J. Wu and H. Zhang, *J. Am. Chem. Soc.*, 2020, **142**, 8953–8961.
35 C. Liu, Q. Sun, L. Lin, J. Wang, C. Zhang, C. Xia, T. Bao, J. Wan, R. Huang, J. Zou and C. Yu, *Nat. Commun.*, 2020, **11**, 4971.
36 N. Kurono, K. Arai, M. Uemura and T. Ohkuma, *Angew. Chem., Int. Ed.*, 2008, **47**, 6643–6646.
37 W. B. Wu, J. S. Yu and J. Zhou, *ACS Catal.*, 2020, **10**, 7668–7690.
38 X. P. Zeng, J. C. Sun, C. Liu, C. B. Ji and Y. Y. Peng, *Adv. Synth. Catal.*, 2019, **361**, 3281–3305.
39 M. North, M. Omedes-Pujol and C. Young, *Biomol. Chem.*, 2012, **10**, 4289–4298.
40 Z. Zhang, J. Chen, Z. Bao, G. Chang, H. Xing and Q. Ren, *RSC Adv.*, 2015, **5**, 79355–79360.
41 H. An, J. Zhang, S. Chang, Y. Hou and Q. Zhu, *Inorg. Chem.*, 2020, **59**, 10578–10590.
42 H. F. Yao, Y. Yang, H. Liu, F. G. Xi and E. Q. Gao, *J. Mol. Catal. A: Chem.*, 2014, **394**, 57–65.
43 Y. Jiang, J. Xu, Z. Zhu, C. Jiang, L. Ma, H. Wang, L. Wang and Y. Fan, *Inorg. Chim. Acta*, 2020, **510**, 119735.
44 D. Kumar, A. P. Prakasham, M. K. Gangwar and P. Ghosh, *Inorg. Chim. Acta*, 2019, **495**, 119003.
45 L. M. Aguirre-Díaz, M. Iglesias, N. Snejko, E. Gutiérrez-Puebla and M. Á. Monge, *CrystEngComm*, 2013, **15**, 9562–9571.